Earth Planet. Sci. Lett. 624 (2023) 118446

Contents lists available at ScienceDirect

Earth and Planetary Science Letters

journal homepage: www.elsevier.com/locate/epsl

Large sulfur isotope fractionation during abiotic consumption of hydrogen sulfide after cessation of bacterial growth in batch culture experiments of sulfate reducing bacteria

Fumihiro Matsu'ura [a,b,*], Hiroko Makita [c,d], Ken Takai [d], Mayuko Nakagawa [b,e], Yuichiro Ueno [b,d,e]

[a] International Center for Isotope Effects Research, Nanjing University, No.163 Xianlin Avenue, Qixia District, Nanjing, Jiangsu Province 210023, China
[b] Earth-Life Science Institute (ELSI), Tokyo Institute of Technology, 2-12-1 Ookayama, Meguro-ku, Tokyo 152-8550, Japan
[c] Department of Ocean Sciences, Tokyo University of Marine Science and Technology, 4-5-7 Konan, Minato-ku, Tokyo 108-8477, Japan
[d] Institute for Extra-Cutting-Edge Science and Technology Avant-Garde Research, (X-star), Super-cutting-edge Grand and Advanced Research (SUGAR) Program, Japan Agency for Marine-Earth Science and Technology (JAMSTEC), Yokosuka, 237-0061, Japan
[e] Department of Earth and Planetary Sciences, Tokyo Institute of Technology, Meguro, Tokyo 152-8551, Japan

ARTICLE INFO

Keywords:
Large sulfur isotope fractionation
Sulfate reducing bacteria
Abiotic sulfide consumption
Organic sulfur
Sulfide mineral precipitation

ABSTRACT

Microbial sulfate reduction is a key process in the oceanic sulfur cycle and imparts a large sulfur isotope fractionation. The mechanism of sulfur isotope fractionation during microbial sulfate reduction has been studied from the geochemical and biochemical aspects since the 1950s. Recently, however, the large sulfur isotope fractionation, exceeding 47‰, has been observed in some pure culture experiments of sulfate reducing bacteria and the tentative understanding of microbial sulfur isotope fractionation has not well explained the mechanism. Here we quantified growth phase dependent sulfur isotope fractionation of a type sulfate reducer *Desulfovibrio desulfuricans* (DSM642) and revealed that the magnitude of isotope fractionation increased from -13.4 ± 3.6‰ in early exponential phase to -65.9 ± 21.0‰ in later exponential phase having clear negative correlation with cell specific sulfate reduction rate. Our results show the importance of cells growth phase and states that control cell specific sulfate reduction rate and sulfur isotope fractionation. Although microbial sulfate reduction likely continued to stationary phase of cells, microbial sulfur isotope fractionation could not be quantified because of the decreasing total dissolved sulfide (ΣH_2S: H_2S, HS^-, and S^{2-}) concentration after stationary phase. A non-microbial ΣH_2S-consuming reaction is interpreted to have occurred during the stationary phase and this had large sulfur isotope fractionations, -10.5 ± 1.1‰ and -45.6 ± 12.4‰. Besides, the non-microbial ΣH_2S-consuming reaction decreased $\Delta^{33}S$' value of the ΣH_2S. While the end-product of the non-microbial ΣH_2S-consuming reaction in the stationary phase remains unidentified, we observed precipitates of some sulfide minerals and organic sulfur in the stationary phase media. Regardless of the end-product, the reaction increases the sulfur isotopic composition of dissolved ΣH_2S, which can account for the high sulfur isotopic compositions of ΣH_2S compared to pyrite and organic sulfur observed in some modern marine sediments.

1. Introduction

Sulfur isotope fractionation by sulfate-reducing microbes is a key to understand biogeochemical sulfur cycle in the past and present Earth (Johnston, 2011). The sulfur isotope fractionation has been well known to change with sulfate concentration, species and concentration of electron donor, temperature, and so on (Sim et al., 2011a, 2011b; Leavitt et al., 2013; Bradley et al., 2016; Pellerin et al., 2020). However, the mechanism of the sulfur isotope fractionation has not been fully understood despite of many studies conducted (Sim et al. 2017; Bertran et al., 2018).

The mechanism has been discussed based on the steady state model developed by Rees (1973). The steady state model provides an insight that the net sulfur isotope fractionation during microbial sulfate

* Corresponding author at: International Center for Isotope Effects Research, Nanjing University, No.163 Xianlin Avenue, Qixia District, Nanjing, Jiangsu Province 210023, China.
E-mail address: matsuura.f@nju.edu.cn (F. Matsu'ura).

https://doi.org/10.1016/j.epsl.2023.118446
Received 8 June 2022; Received in revised form 13 October 2023; Accepted 15 October 2023
Available online 31 October 2023

reduction approaches the equilibrium isotope fractionation of sulfate and total dissolved sulfide (ΣH_2S: H_2S, HS^-, and S^{2-}) at ambient temperature when the rates of all intracellular enzymatic reactions become slow enough to be approximated as reaching equilibrium. The results of incubation experiments by Sim et al. (2011a) provided a good fit to the steady state model that the fractionations obtained from their experiments approached the equilibrium value at room temperature. However, the sulfur isotope fractionation and reaction at each enzymatic step have been just indicated and the whole processes and interactions of each enzymatic step have not been completely understood (Santos et al., 2015; Leavitt et al., 2019).

Recently Sim et al. (2017) for the first time indicated growth-phase-dependent concentration and isotopic composition of intracellular sulfur species, and suggested that a closed system effect on the intracellular sulfate would be important to account for the sulfur isotope fractionation of microbial sulfate reduction. Although growth phases and states of microbes alter the chemical composition of intracellular sulfur species, only a few studies documented the influence of the growth phases and states on sulfur isotope fractionation during microbial sulfate reduction (Matsu'ura et al., 2016a; Pellerin et al., 2018). The small amount of ΣH_2S produced during stationary phase (the stationary phase is defined as a growth phase where cell growth rate is null) of microbial growth may have imposed a limitation on quantifying the isotope fractionation during maintenance metabolism especially in previous batch culture experiments. Here, we carried out batch type glucose culture experiment of *Desulfovibrio desulfuricans* (DSM642) to quantify sulfur isotope fractionation during stationary phase. We found a drastic change of the sulfur isotope fractionation from early to late exponential cells (the exponential phase is defined as a growth phase where cell numbers increase exponentially with constant growth rate), although the much lower ΣH_2S concentration during the stationary phase prevented us from quantifying the sulfur isotope fractionation during stationary phase. Instead, we found that non-microbial ΣH_2S-consuming reactions became dominant during the stationary phase, which imparts large sulfur isotope fractionations and increases the sulfur isotopic composition of ΣH_2S. The ΣH_2S-consuming reaction can account for high $\delta^{34}S$ values of ΣH_2S compared to pyrite or organic sulfur observed in some modern marine sediments.

2. Method

2.1. Batch culture experiments

We used a sulfate-reducing bacterium, *Desulfovibrio desulfuricans* (DSM 642) for the batch culture experiments in the same as Matsu'ura et al., (2016a). We conducted 2 series of experiments (series-1 and series-2) for isotope analysis and 1 series of supplemental experiments (series-3: see supplemental information) for detailed chemical analysis and microscopic observation of precipitates in incubation media. We prepared 3 L of medium and about 30 bottles of 100 ml glass vials for each series of experiment. We named each vial as A-1 to J-3 for the series-1 experiment and A'-1 to H'-3 for the series-2 experiment (Tables S1 and S2). Three vials were harvested at each collection time for both series of experiments. In each glass vial, 40 mL of culture medium for the sulfate reducing bacteria (SRB) [modified DSMZ 63] was injected, and purged with N_2 gas. The vial was plugged with a butyl rubber stopper. Modified DSMZ 63 contains K_2HPO_4, 0.5 g; NH_4Cl, 1.0 g; Na_2SO_4, 1.0 g; $CaCl_2 \times 2H_2O$, 0.1 g; $MgSO_4 \times 7H_2O$, 2.0 g; D(+) glucose, 2.7 g; yeast extract, 1.0 g; resazurin, 1.0 mg; ascorbic acid, 0.1 g; Na-thioglycolate, 0.1 g; distilled water, 1 L. The pH value was adjusted at 7.0. Before adding ascorbic acid and Na-thioglycolate, the 3L medium was autoclaved for degassing, which may have resulted in some water loss due to evaporation. Glucose was used both as an electron donor and as a carbon source. After autoclaving and storing the glass vials at experimental temperature, 30 °C, 100 μL of bacterial culture was inoculated into fresh medium of all 30 vials except for 3 control samples to start experiment. The inoculum of sulfate-reducing bacterium was pre-cultivated in the same medium at 30 °C. Series-1 experiment was conducted without shaking and series-2 experiment was conducted with shaking at 180 rpm. The shaking experiment was conducted to confirm the results of Matsu'ura (2016b).

2.2. Cell growth and chemical analyses

Growth of *D. desulfuricans* (DSM642) was measured by direct cell counting after staining with 4,6-diamidino-2-phenylindole (DAPI) using a Leica AF6000 advanced fluorescence imaging system with Leica DM5500B microscope. In series-1 experiment, cell counting was conducted using 100 μL of medium of harvesting 2 vials (Table S1). In series-2 experiment, cell counting was conducted using 100 μL of medium of vials prepared for cell counting, H'-1 and H'-2 (Table S1).

Cultures were collected alphabetically at 21, 43, 70, 140, 360, 645, and 1801 h after inoculation of series-1 experiment and at 20, 44, 70, 116, 210, 402, and 760 h after inoculation of series-2 experiment (Table S2). ΣH_2S concentration was analyzed for all three vials at each collection time, and sulfate concentration, isotopic composition of sulfate and ΣH_2S were analyzed for 2 of 3 vials at each collection time.

ΣH_2S concentration was determined by the colorimetric methylene-blue method (Cline, 1969) with 400 μL of each collected medium filtered through 0.22 μm syringe filter, and the uncertainties were based on the method of linear regression. ΣH_2S in each vial was collected as silver sulfide by following procedure. At first 1 mL of 45.6 mM of alkaline zinc acetate solution was added to each vial to precipitate ΣH_2S as ZnS and terminate cell activity, followed by injection of 1 mL of 6N HCl to the vial to acidify the medium and convert ZnS to H_2S. The H_2S gas was scrubbed with distilled water by purging with N_2 gas and finally trapped as Ag_2S by reaction with silver nitrate solution. After completion of purging H_2S, 1 mL of 1 M $BaCl_2$ solution was added to the vial to collect sulfate as $BaSO_4$. The collected Ag_2S and $BaSO_4$ were then washed by repeated centrifugation using distilled water. The collected $BaSO_4$ was weighed and further reduced to H_2S by the reaction with tin (II)-Strong phosphoric acid solution (Kiba et al., 1955). The evolved H_2S was collected as Ag_2S in the same way as described above. Sulfate concentration was determined from the weight of collected $BaSO_4$ with the uncertainty of 3 % for series-1and 1.5 % for series-2 experiments (1σ).

Cell specific sulfate reduction rates (fmol/cell/day) are described as Eq. (1) (Detmers et al., 2001)

$$csSRR = (M_{H2S(i+1)} - -M_{H2S(i)}) / \left(\left(\left(C_{(i+1)} + C_{(i)} \right) / 2 \right) \times \left(T_{(i+1)} - T_{(i)} \right) \right). \quad (1)$$

here C and M_{H2S} refer to cell density and concentration of ΣH_2S at *i*th and *(i+1)*th of time of harvesting vials. The uncertainties on all the calculated values in this study are denoted as σ and calculated by analytical values, analytical uncertainties, and equation of uncertainty propagation (eqs. S1, S2, S3, S5, S7, S9, and S10), respectively.

2.3. Cell free experiments

A cell free experiment was carried out to confirm whether the decreasing ΣH_2S in the stationary phase was related to microbial activity or not. In addition, a supplemental cell free experiment was conducted to confirm whether glucose was involved in the reaction (see supplemental information). To prepare the ΣH_2S solution, 0.312 g of $Na_2S \bullet 9H_2O$ and resazurin was dissolved in 300 mL of degassed distilled water while continuing N_2 purging of the water. The pH was adjusted to 7.0. The N_2 purge of the solution was continued for 40 min after pH adjustment to deoxidize the solution, although at the same time H_2S gas leaked from the solution. After the N_2 purge, 5 mL of the ΣH_2S solution was added to each of 6 uninoculated medium, which are same as used in series-2 experiment. The 6 vials were immediately set to incubator at 30 °C without shaking. Two vials were collected at each collection time

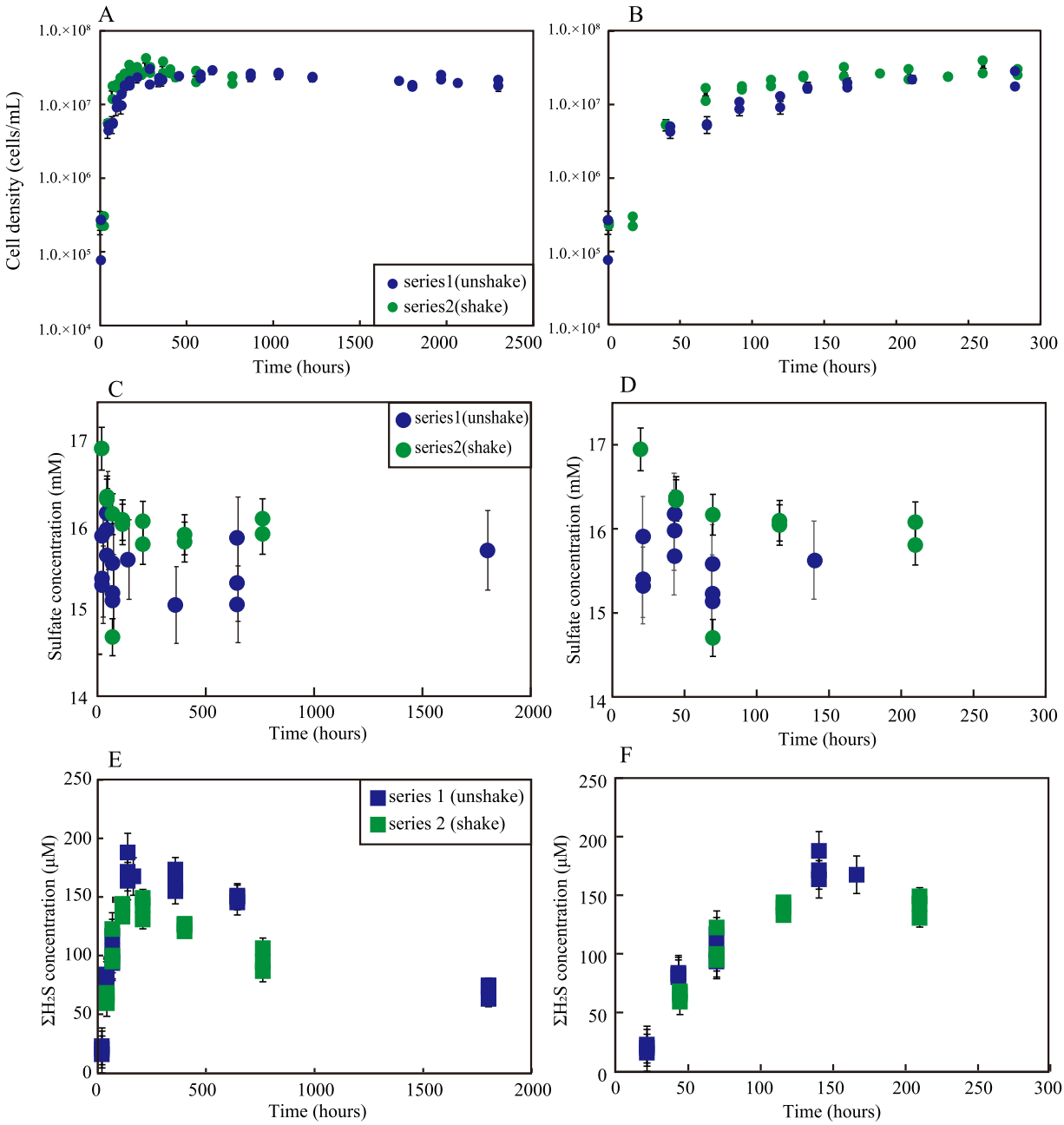

Fig. 1. Cell densities, sulfate concentrations, and ΣH_2S concentrations of series-1 and series-2 experiments. (A) Cell growth of entire series of experiments. (B) Cell growth of early stage of incubation. (C) Sulfate concentration throughout the experiments. (D) Sulfate concentration of early stage of the incubation. (E) ΣH_2S concentration throughout the experiments. (F) ΣH_2S concentration of early stage of the incubation. Blue and green plots are series-1 and series-2 experiments, respectively.

of 22 h, 335 h, and 743 h after setting the vials in the incubator. ΣH_2S concentration of each collected medium was determined same as described above. The pH of all collected medium was checked and ranged from 6.62 to 6.80.

2.4. Sulfur isotope analyses

Multiple sulfur isotope analysis was carried out via a flash heating method with CoF_3 (Ueno et al., 2015). The Ag_2S samples from ΣH_2S and sulfate were wrapped with CoF_3 in a thin foil that consists of iron-nickel-cobalt alloy (pyrofoil) and heated to 590 °C for 3 seconds by Curie-point pyrolyzer (JHP-22, Japan Analytical Industry Co., Ltd.). The Ag_2S was converted to SF_6, followed by collection in a cold trap at -196 °C (Trap-1) by using liquid nitrogen. Subsequently, HF was removed by a cold trap maintained at -90 °C. The pre-treated SF_6 was further purified by gas chromatography (GC8A, Shimadzu), equipped with the first 4 m column packed with Porapack-Q (1/8″ OD, 80-100 mesh) connected with the second 3 m Molecular Sieves 5A column (1/8″ OD, 60-80 mesh) at 50 °C oven temperature and a 25 mL/min of He flow rate. Purified SF_6 was introduced into a mass spectrometer (Thermo Fisher Scientific, MAT253) and abundances of $^{32}SF_5^+$, $^{33}SF_5^+$, $^{34}SF_5^+$, and $^{36}SF_5^+$ were measured in a dual inlet mode.

Sulfur isotopic compositions are reported as below.

$$\delta^{3x}S = \left({}^{3x}R_{sample}/{}^{3x}R_{standard} - 1\right) \times 1000 \quad (2)$$

$$\delta^{3x}S' = ln\left({}^{3x}R_{sample}/{}^{3x}R_{standard}\right) \times 1000 \quad (3)$$

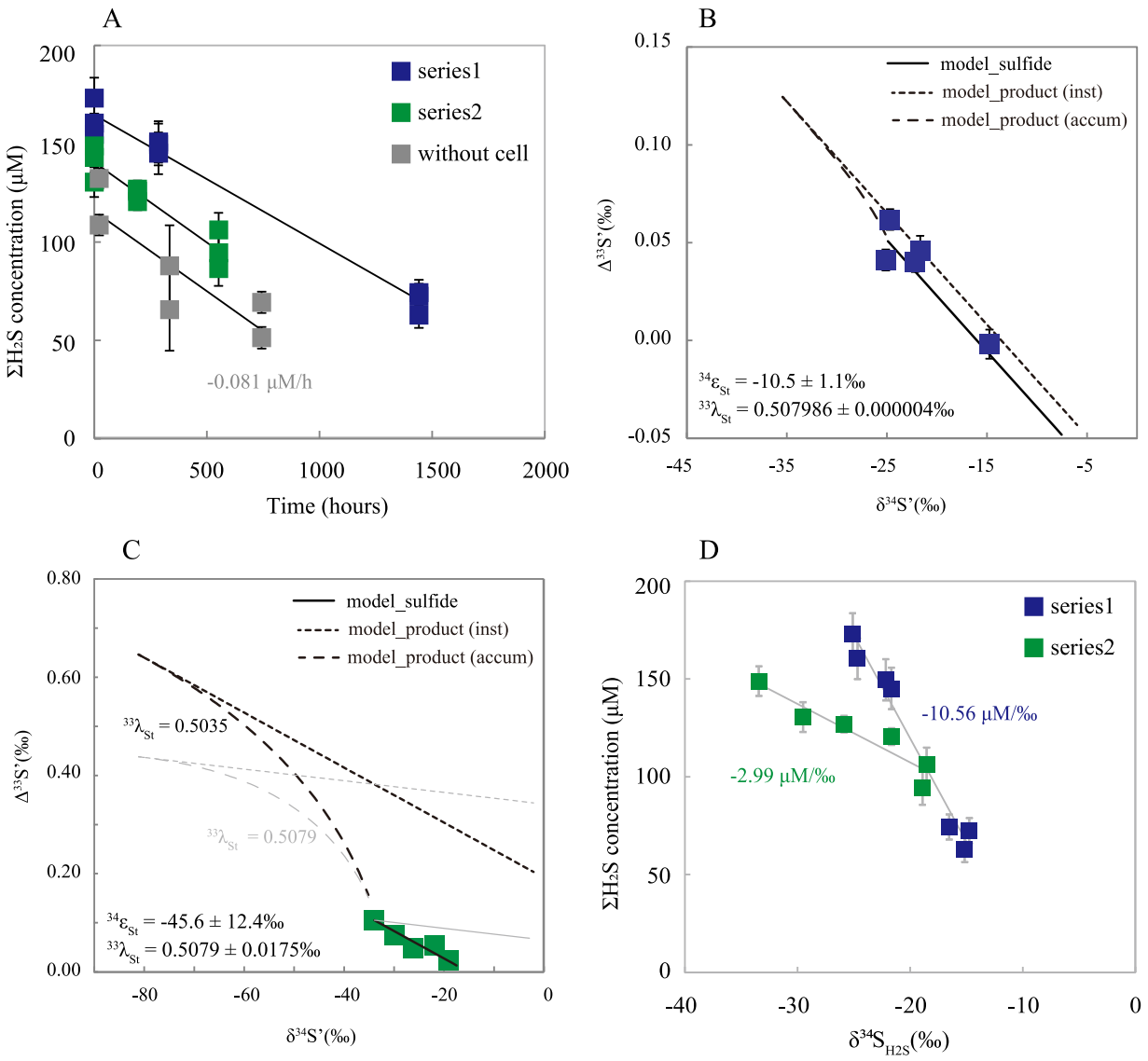

Fig. 2. (A) ΣH_2S concentration in the stationary phase cells and the cell free experiment. The time of 360 h in series-1 experiment and 210 h in series-2 experiments are set to 0h for the two series of experiments. The ΣH_2S decreasing rate of the cell free experiment was obtained from the slope of the linear regression line as -0.081 μM/h. (B) Evolution of $\delta^{34}S'$ and $\Delta^{33}S'$ values in the stationary phase in series-1 experiment with calculated Rayleigh distillation equation model. The data align well with model calculation. (C) Evolution of $\delta^{34}S'$ and $\Delta^{33}S'$ values in the stationary phase in series-2 experiment with calculated Rayleigh distillation equation model. The data deviate largely from the model calculation with original $^{34}\varepsilon_{st}$ and $^{33}\lambda_{st}$ values, -45.6‰ and 0.5079, respectively (gray lines). (D) Cross plots of ΣH_2S concentration and $\delta^{34}S_{SO4}$ value in the stationary phase of the two series of experiments. The calculated slope of series-2 experiment (-2.99 μM/‰), was used for the calculation of the impact of the ΣH_2S-consuming reaction on the $^{34}\varepsilon_{SR}$ values (see supplement).

$$\Delta^{33}S' = \delta^{33}S' - 0.515 \times \delta^{34}S' \quad (4)$$

where 3x denotes 33 or 34, $^{3x}R_{sample}$ denotes isotopic ratio of samples ($^{3x}S/^{32}S$). All values are reported relative to V-CDT assuming that IAEA-S1 has a composition on the V-CDT scale of $\delta^{34}S$ = -0.3‰ and $\Delta^{33}S'$ = +0.100‰ (Ding et al., 2001; Ono et al., 2006). The analytical uncertainty (1σ) on $\delta^{34}S$ and $\Delta^{33}S'$ for series-1 experiment are ±0.78‰ and ± 0.005‰ and are ±0.26‰ and ± 0.009‰ for series-2 experiment. The uncertainties are based on replicate analyses of IAEA-S1.

2.5. Isotope fractionation calculations

In this study, sulfur isotope fractionation of microbial sulfate reduction in exponential phase is described as

$$^{3x}\varepsilon_{SR} = 1000 \times \left(^{3x}\alpha_{SR} - 1\right) \quad (5)$$

where $^{3x}\alpha_{SR}$ is sulfur isotope fractionation factor of microbial sulfate reduction. The sulfur isotope fractionation factor is described as

$$^{3x}\alpha_{SR} = {}^{3x}R_{H2S\_Inst} / {}^{3x}R_{SO4} = \left(\delta^{3x}S_{H2S\_Inst} + 1000\right) \Big/ \left(\delta^{3x}S_{SO4} + 1000\right). \quad (6)$$

where $^{x}R_{H2S\_Inst}$ and $\delta^{x}S_{H2S\_Inst}$ denote isotopic ratio and isotopic composition of ΣH_2S produced between *i*th and *(i+1)*th of time of harvesting vials, respectively. The $^{3x}R_{SO4}$ and $\delta^{3x}S_{SO4}$ denote the average of isotopic ratio and isotopic composition of sulfate at the *(i+1)*th harvesting vials. Equations for calculating the values and uncertainties on $\delta^{3x}S_{H2S\_Inst}$, $\delta^{3x}S_{SO4}$, and $\delta^{3x}S_{TS}$ (isotopic composition of total sulfur in each vial) are described in supplemental information.

Sulfur isotope fractionation of the ΣH_2S-consuming reaction in stationary phase is described as

$$^{3x}\varepsilon_{St} = 1000 \times \left(^{3x}\alpha_{St} - 1\right) \quad (7)$$

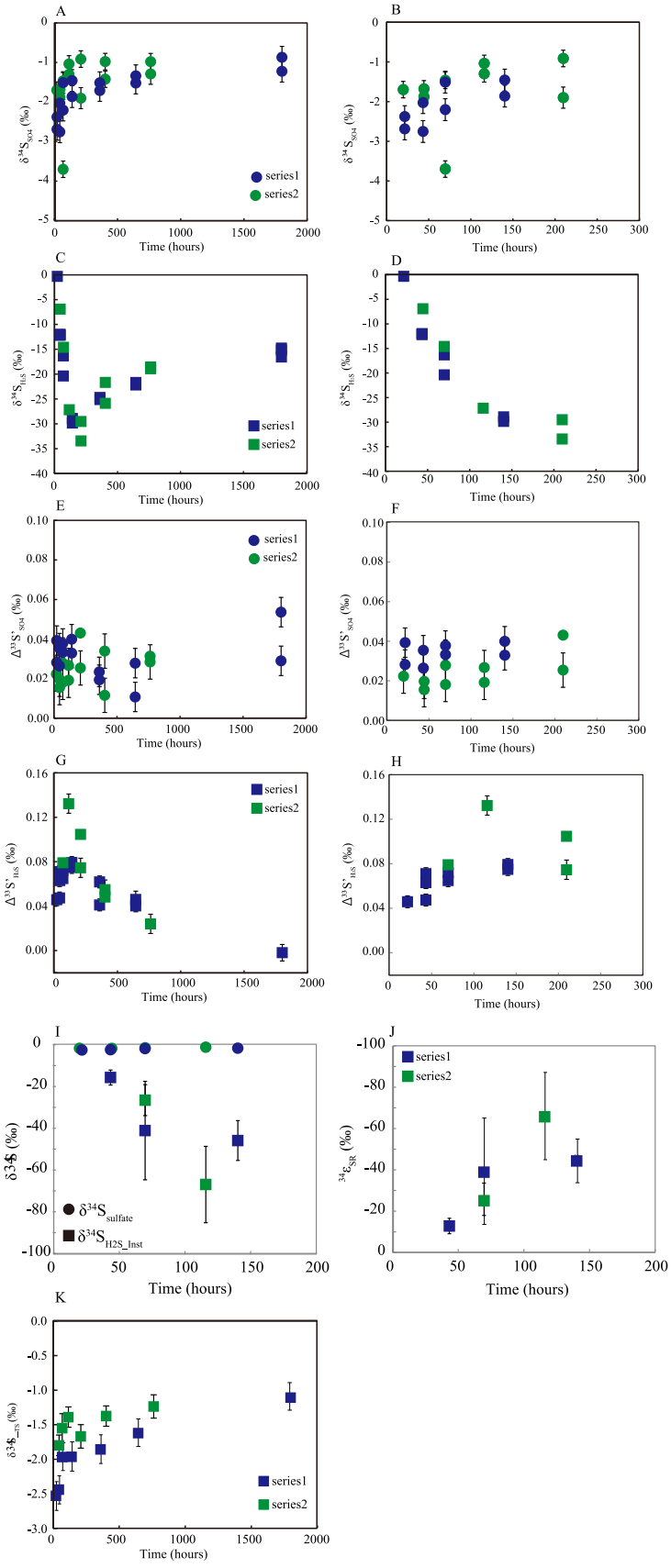

(caption on next page)

Fig. 3. Temporal variations of the isotopic compositions of sulfate and ΣH_2S, sulfur isotope fractionation of microbial sulfate reduction in exponential phase—$^{34}\varepsilon_{SR}$—, and isotopic composition of total sulfur—$\delta^{34}S_{TS}$—. (A) Temporal variation of the $\delta^{34}S_{SO4}$ values throughout the experiments. (B) Enlarged figure of (A) in early stage of the experiments. (C) Temporal variation of the $\delta^{34}S_{H2S}$ values throughout the experiments. (D) Enlarged figure of (C) in early stage of the experiments. (E) Temporal variation of the $\Delta^{33}S'_{SO4}$ values throughout the experiments. (F) Enlarged figure of (E) in early stage of the experiments. (G) Temporal variation of the $\Delta^{33}S'_{H2S}$ values throughout the experiments. (H) Enlarged figure of (G) in early stage of the experiments. (I) Temporal variations of $\delta^{34}S_{SO4}$ and $\delta^{34}S_{H2S\_Inst}$ in the exponential phase of the two series experiments. Circles and squares denote $\delta^{34}S_{SO4}$ and $\delta^{34}S_{H2S\_Inst}$, respectively. Blue and green colors denote series-1 and series-2 experiments, respectively. The $^{34}\varepsilon_{SR}$ value was obtained from these values. (J) Temporal variation of $^{34}\varepsilon_{SR}$ value in the exponential phase of the two series of experiments. (K) Temporal variation of the $\delta^{34}S_{TS}$ values throughout the experiments. Blue and green plots are series-1 and series-2 experiments, respectively.

where $^{3x}\alpha_{St}$ is sulfur isotope fractionation factor of the ΣH_2S-consuming reaction and described as

$$^{3x}\alpha_{St} = {}^{3x}R_{product} / {}^{3x}R_{H2S}. \quad (8)$$

where $^{3x}R_{product}$ and $^{3x}R_{H2S}$ denote isotopic ratio of the product of the stationary phase reaction and of ΣH_2S, respectively. The isotope fractionation factor and the uncertainty of the reaction of the stationary phase is calculated from Rayleigh distillation equation described as

$$\delta^{3x}S'_{H2S(j)} = \delta^{3x}S'_{H2S(j-0)} + 1000 \times \left({}^{3x}\alpha_{St} - 1\right) \times lnf \quad (9)$$

where $\delta^{3x}S'_{H2S(j)}$ denotes the isotopic composition of ΣH_2S in each collected sample during the stationary phase. The *f* value denotes fraction of ΣH_2S concentration relative to the initial concentrations of ΣH_2S in stationary phase of each series of experiment; the initial ΣH_2S concentrations are fixed as the concentration of E-2 (173.1 μM) in series-1 experiment and E'-2 (148.9 μM) in series-2 experiment. The linear regression of the plots of $\delta^{3x}S'_{H2S(j)}$ and ln*f* provide the isotope fractionation factor, the isotopic composition of initial ΣH_2S ($\delta^{3x}S'_{H2S(j-0)}$), and uncertainties of them (Eq. 9, Fig. S1). Because of the large uncertainty on the ln*f* value, we employed straight line fitting with uncertainties present in both the x and y variables (Fig. S1, see Appendix A in Matsu'ura et al., 2016a).

The mass dependence of the isotope fractionation during the reaction of the stationary phase is described as

$$^{33}\lambda_{St} = ln\left({}^{33}\alpha_{St}\right) / ln\left({}^{34}\alpha_{St}\right). \quad (10)$$

The equation of calculation on the uncertainty of $^{33}\lambda_{St}$ value (including the difference of the calculation method from previous studies) is described in supplemental information.

3. Results

3.1. Cell growth

In the series-1 experiment, cell density increased from 2.0×10^5 cells/mL at inoculation to 2.2×10^7 cells/mL by 211 h and became almost constant after 211 h (Fig. 1; Table S1). In the series-2 experiment, cell density increased from 2.0×10^5 cells/mL at 17 h to 2.9×10^7 cells/mL at 164 h, fluctuated around 3.0×10^7 cells/mL until 401 h, and decreased to 2.1×10^7 cells/mL at 760 h (Fig. 1; Table S1). Cell growth rate during the exponential phase in series-2 experiment is higher than that of the series-1 experiment (Fig. 1; Table S1).

3.2. Concentration of sulfate and ΣH_2S

The sulfate concentration was between 15 mM and 16 mM throughout in the series-1 experiment (Fig. 1, Table S2). In the series-2 experiment, the sulfate concentration decreased from 16.9 mM at 20 h to 16.0 mM at 116 h and became almost constant after 116 h. The sulfate concentration of C'-1 (a vial collected at 70 h of series-2 experiment) was 14.7 mM, which is clearly low compared to other samples (Fig. 1, Table S2).

The average ΣH_2S concentration increased from 19.3 ± 9.1 μM at 21 h to 174.2 ± 9.3 μM at 140 h during the exponential phase and was deceasing after 140 h to 69.9 ± 3.7 μM at 1801 h during the stationary phase in series-1 experiment (Fig. 1, Table S2). The average ΣH_2S concentration increased from 64.3 ± 6.3 μM at 44 h to 139.0 ± 2.9 μM at 116 h during the exponential phase and started decreasing after 210 h to 95.7 ± 5.1 μM at 762 h during the stationary phase in series-2 experiment (Fig. 1, Table S2).

The average ΣH_2S concentration decreased from 120.5 ± 3.7 μM at 22 h to 60.3 ± 3.9 μM at 743 h in the cell free experiment (Fig. 2A). The decreasing ΣH_2S concentration in the cell free experiment is consistent with those of the stationary phase of the series-1 and -2 experiments (Fig. 2A).

3.3. $\delta^{34}S$ values of sulfate and ΣH_2S

The average $\delta^{34}S$ value of sulfate in the series-1 experiment increased from -2.5 ± 0.2‰ at 21 h to -1.7 ± 0.2‰ at 140 h during the exponential phase and continued increasing to -1.0 ± 0.2‰ at 1801 h during the stationary phase (Fig. 3A, Table S2). The average $\delta^{34}S$ value of sulfate in the series-2 experiment increased from -1.7 ± 0.2‰ at 20 h to -1.2 ± 0.15‰ at 116 h during the exponential phase and became almost constant after 116 h (Fig. 3A, Table S2). The $\delta^{34}S$ value of C'-1 was - 3.7‰, which is low compared to other samples (Fig. 3B, Table S2).

The average $\delta^{34}S$ value of ΣH_2S in the series-1 experiment decreased from -0.3 ± 0.8‰ at 21 h to -29.4 ± 0.5‰ at 140 h during the exponential phase and was increasing after 140 h to -15.5 ± 0.1‰ at 1801 h during the stationary phase (Figs. 3C and 3D, Table S2). The average $\delta^{34}S$ value of ΣH_2S in the series-2 experiment decreased from -6.9 ± 0.3‰ at 44 h to -27.2 ± 0.3‰ at 116 h during the exponential phase and was increasing after 210 h to -18.7 ± 0.2‰ at 762 h during the stationary phase (Figs. 3C and 3D, Table S2).

The $\delta^{34}S_{TS}$ value continuously increased from -2.5 ± 0.2‰ at 21 h to -1.1 ± 0.2‰ at 1801 h concomitant with the increase of $\delta^{34}S$ value of sulfate in series-1 experiment (Fig. 3K). The $\delta^{34}S_{TS}$ value in series-2 experiment also continuously increased from -1.8 ± 0.2‰ at 44 h to -1.2 ± 0.2‰ at 762 h (Fig. 3K).

3.4. $\Delta^{33}S'$ values of sulfate and ΣH_2S

The average $\Delta^{33}S'$ value of sulfate in the series-1 experiment was almost constant at about +0.035‰ until 140 h and then decreased to +0.020‰ at 360 h followed by an increase to +0.041‰ at 1801 h (Figs. 3E and 3F, Table S2). The average $\Delta^{33}S'$ value of sulfate in the series-2 experiment was almost constant at about +0.020‰ until 116 h, which is lower than that of the series-1 experiment in the exponential phase (Figs. 3E and 3F, Table S2).

The average $\Delta^{33}S'$ value of ΣH_2S in the series-1 experiment increased from +0.046 ± 0.005‰ at 21 h to +0.077 ± 0.004‰ at 140 h during the exponential phase and was decreasing after 140 h to -0.002 ± 0.007‰ at 1801 h during the stationary phase (Figs. 3G and 3H, Table S2). The average $\Delta^{33}S'$ value of ΣH_2S in the series-2 experiment increased from +0.079‰ at 70 h to +0.132 ± 0.009‰ at 116 h during the exponential phase and was decreasing after 210 h to +0.024 ± 0.009‰ at 762 h during the stationary phase (Figs. 3G and 3H, Table S2).

Table 1
Calculated sulfur isotope fractionations and csSRRs of both series of experiments. The time of *(i+1)*th of harvesting vials is used to express the time interval between ith and *(i+1)*th collection time.

	csSRR (fmol/cell/day)	σ_{csSRR} (fmol/cell/day)	$^{34}\varepsilon_{SR}$ (‰)	$\sigma^{34}\varepsilon_{SR}$ (‰)
Series-1 43 h	28.1	7.2	-13.4	3.6
Series-1 70 h	4.1	2.3	-39.3	25.6
Series-1 140 h	2.1	0.5	-44.3	10.5
Series-2 70 h	4.0	1.1	-25.1	7.4
Series-2 116 h	1.0	0.3	-65.9	21.0

3.5. Sulfur isotope fractionation

3.5.1. Sulfur isotope fractionation during microbial sulfate reduction: $^{34}\varepsilon_{SR}$

The $\delta^{34}S_{H2S\_Inst}$ decreased from -15.7 ± 3.6‰ at 43 h to -45.9 ± 9.6‰ at 140 h in the series-1 experiment (Fig. 3I). The magnitude of $^{34}\varepsilon_{SR}$ value calculated from the $\delta^{34}S_{H2S\_Inst}$ of the series-1 experiment increased from -13.4 ± 3.7‰ at 43 h to -44.3 ± 10.5‰ at 140 h (Fig. 3J; Table 1). The $\delta^{34}S_{H2S\_Inst}$ decreased from -26.6 ± 7.4‰ at 70 h to -67.0 ± 18.3‰ at 116 h in the series-2 experiment (Fig. 3I). The magnitude of $^{34}\varepsilon_{SR}$ value calculated from the $\delta^{34}S_{H2S\_Inst}$ of the series-2 experiment increased from -25.1 ± 7.8‰ at 70 h to -65.9 ± 21.0‰ at 116 h (Fig. 3J; Table 1).

3.5.2. Sulfur isotope fractionation of the ΣH_2S-consuming reaction in stationary phase: $^{34}\varepsilon_{St}$

The calculated $^{34}\varepsilon_{St}$ and $\delta^{34}S'_{H2S(j\text{-}0)}$ values in the series-1 experiment are -10.5 ± 1.1‰ and -24.8 ± 0.7‰, respectively (Fig. S1); the calculated $^{34}\varepsilon_{St}$ and $\delta^{34}S'_{H2S(j\text{-}0)}$ values in the series-2 experiment are -45.6 ± 12.4‰ and -34.2 ± 2.7‰, respectively (Fig. S1). The mass dependence of the reaction ($^{33}\lambda_{St}$) in the series-1 and -2 experiments are 0.507986 ± 0.000004 and 0.5079 ± 0.0175, respectively (Fig. 2). In the series-1 experiment, the $\delta^{34}S'_{H2S}$ and $\Delta^{33}S'_{H2S}$ values of samples fit well with the model of Rayleigh distillation equation with the obtained values of $^{34}\varepsilon_{St}$ = -10.5‰, $^{33}\lambda_{St}$ = 0.507986, $\delta^{34}S'_{H2S(j\text{-}0)}$ = -24.8‰, and $\Delta^{33}S_{H2S(j\text{-}0)}$' = +0.051‰ (Fig. 2B). In the series-2 experiment, the $\delta^{34}S'_{H2S}$ and $\Delta^{33}S'_{H2S}$ values of samples deviate from the model of Rayleigh distillation equation with the obtained values of $^{34}\varepsilon_{St}$ =-45.6‰, $^{33}\lambda_{St}$ = 0.5079, $\delta^{34}S'_{H2S(j\text{-}0)}$ = -34.2‰, and $\Delta^{33}S_{H2S(j\text{-}0)}$' = +0.105‰ (gray lines in Fig. 2C). The black lines in Fig. 2C were annotated with the model calculation with modified $^{33}\lambda_{St}$ value as 0.5035 to adjust the data. The difference of slope of the linear regression line of ΣH_2S concentration and $\delta^{34}S_{H2S}$ value in the stationary phase shows the isotope fractionation factors of the two series experiments are different (Fig. 2D).

4. Discussion

4.1. Inconsistent $\delta^{34}S_{TS}$ values in exponential and stationary phase

The $\delta^{34}S_{TS}$ values in the exponential phase increased c.a. 0.5‰ in both series of experiments (Fig. 3K). If we could quantify concentration and isotopic composition of all sulfur species in the vials correctly, $\delta^{34}S_{TS}$ must have been constant. In the series-1 experiment, ΣH_2S concentration and $\delta^{34}S_{SO4}$ increased c.a. 170 μM and 1‰, respectively (Figs. 1E and 3A), which shows clear evidence of microbial sulfate reduction. On the other hand, sulfate concentration was almost constant throughout the experiment, which indicates the analytic uncertainty on the sulfate concentration is too large to quantify the decreased sulfate concentration for series-1 experiment (Fig. 1C). The uncertainty on the sulfate concentration of the series-1 experiment is likely attributed to extraction of aliquot of medium for cell counting before chemical analysis (Table S1). The extraction of medium is unlikely to affect the ΣH_2S concentration because we employed colorimetric method. In the series-2 experiment, the sulfate concentration decreased from 16.9 mM to 16.0 mM during the exponential phase (Fig. 1C). Besides, the sulfate concentration analyzed by ion-chromatography in the series-3 experiment decreased from 15.6 mM to 15.2 mM during the exponential phase (Fig. S2C and S2D). Although the decreased sulfate concentration was μM level in all series experiments, the decreased sulfate concentration was larger than the analyzed ΣH_2S concentration (Figs. 1C and 1E; Figs. S2C and S2E). The discrepancy indicates sulfur reservoirs other than extracellular sulfate and ΣH_2S exist.

Some previous studies advocated the inconsistency of $\delta^{34}S_{TS}$ is owing to cell's internal sulfur reservoir (Rees et al., 1973; Stögbauer et al., 2004). We calculated the mass of the internal sulfur at 70 h of the series-2 experiment where cell density was 1.4×10^7 cells/mL assuming mass of internal sulfur reservoir is 10^{-12} mgS/cell (Rees, 1973). The calculated mass of the internal sulfur reservoir was 0.6 μg, which corresponds to only 0.4 μM of sulfur in the medium. Thus, another sulfur reservoir is required to account for the discrepancy. Previous studies showed accumulation of extracellular intermediate sulfur species such as sulfite or thiosulfate (Chambers and Trudinger, 1979; Davidson et al., 2009). The thiosulfate concentration analyzed in the series-3 experiment using ion-chromatography shows thiosulfate did not increase and was under the detection level in almost all samples (Fig. S3A), which shows thiosulfate cannot account for the mass-imbalance. Finally, we carried out SEM-EDS observation of precipitates in the media of the series-3 experiment. We observed 4 visible grains (>10μm) of zinc sulfide even in an uninoculated medium (Fig. S4A), which of the sulfur source is likely derived from yeast extract and sulfur-containing reducing agent. Although we did not conduct SEM observation for exponential phase samples in the series-1 and -2 experiments, most of the sulfur-containing mineral was considered to be zinc sulfide (Fig. S4B-D). The size and number of the zinc sulfide crystals seems to have increased throughout the experiment (7 visible grains at 476 h and 6 visible grains at 593 h; Fig. S4B-D). However, the calculated amount of one visible ZnS grain assuming the volume of $25^3 \mu m^3$ was only 6.4×10^{-10} mol, which corresponds to 16 nM of sulfur in the medium. Even considering all visible grain in the medium at 476 h (7×40 mL/10 mL = 28), the sulfur in visible ZnS is equivalent to 0.45 μM, which also cannot explain the discrepancy of mass balance. Thus, the mass and isotope imbalances in exponential phase are still elusive. Notably, the ΣH_2S concentration carried over by the 100 μL injection medium was trivial and corresponds to <0.5 μM.

The $\delta^{34}S_{TS}$ value in the stationary phase increased from -1.96 ± 0.2‰ at 140 h to -1.11 ± 0.2‰ at 1801 h in series-1 experiment associated with the increase of $\delta^{34}S_{SO4}$ value (Figs. 3A and 3K). Contrary to the series-1 experiment, the $\delta^{34}S_{TS}$ value in the stationary phase is almost within the error range in series-2 experiment (Fig. 3K). The factor which increases the $\delta^{34}S_{SO4}$ is likely the microbial sulfate reduction in the case of series-1 experiment and the microbial sulfate reduction likely occurred even during the stationary phase cells in the series-1 experiment. However, the occurrence of microbial sulfate reduction is not evident during the stationary phase of the series-2 experiment.

4.2. Sulfur isotope fractionation by microbial sulfate reduction ($^{34}\varepsilon_{SR}$) and cell growth phase and states

The magnitude of microbial sulfur isotope fractionation, $^{34}\varepsilon_{SR}$, and csSRR have a clear negative correlation (Fig. 4; Table 1). The largest $^{34}\varepsilon_{SR}$ value of -65.9 ± 21.0‰ at 116 h of series-2 experiment is achieved when the csSRR was the lowest, 1.0 ± 0.3 fmol/cell/day (Table 1). These were the values that obtained from the latest phase of growth in both the series of experiments. On the other hand, the smallest $^{34}\varepsilon_{SR}$ value, -13.4 ± 3.6‰, was achieved at 43 h of series-1 experiment when the csSRR was the highest, 28.1 ± 7.2 fmol/cell/day (Table 1). Our results show the $^{34}\varepsilon_{SR}$ value varies over 50‰ by changing growth phase and states of cells. The difference of the largest $^{34}\varepsilon_{SR}$ value between the series-1 and -2 experiments was also controlled by csSRR (Fig. 4; Table 1). Since the largest $^{34}\varepsilon_{SR}$ value was different in the two series of experiment, any of the conditions is involved in the difference between

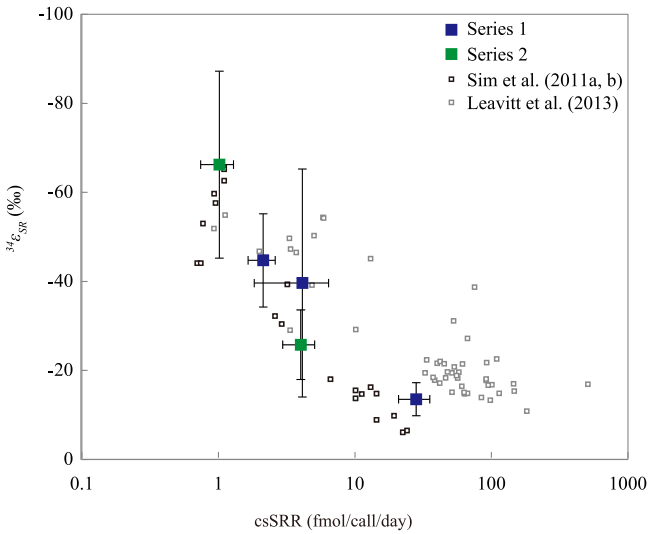

Fig. 4. Sulfur isotope fractionation of microbial sulfate reduction in the exponential phase ($^{34}\varepsilon_{SR}$) and cell specific sulfate reduction rate. The magnitude of $^{34}\varepsilon_{SR}$ value and csSRR have clear negative correlation consistent with previous studies. Blue and green squares denote series-1 and series-2 experiments of this study, respectively. Black and gray small squares denote the data from Sim et al. (2011a, 2011b) and Leavitt et al. (2013), respectively.

the two series of experiments (Fig. 4). The much lower csSRR was observed at 116 h of series-2 (with shaking) experiments than those of the series-1 (without shaking) experiment, which resulted from much higher cell density at that time of series-2 experiments than those of the series-1 experiment (Fig. 1B). Further, total sulfate reduction rate was lower at 116 h of the series-2 experiments than those of the series-1 experiment (Fig. 1F). The shaking condition may have provided a faster cell specific growth rate (Figs. 1A and 1B) and subsequently introduced the faster entry to the stationary phase of growth and sulfate reduction than the static condition, which may have led to the smallest csSRR value at 116 h of the series-2 experiments. The influence of the ΣH_2S-consuming reaction in the stationary phase on the $^{34}\varepsilon_{SR}$ values are trivial and discussed in supplemental information.

Although there is no report that *D. desulfuricans* utilizes glucose as an electron donor and our HPLC-based glucose analysis failed to detect decreasing glucose in the series-3 experiment (Fig. S3B), we confirmed that *D. desulfuricans* oxidized glucose instead of yeast extract as the electron donor in the present study. When *D. desulfuricans* was cultivated in the medium with or without glucose in series-3 experiment, the specific growth rate was greater in the medium with glucose than in the glucose-free medium in series-3 experiment (Figs. S2A and S2B). In addition, we observed all sulfate and glucose were consumed and mM level of ΣH_2S was produced when we modified the inoculum volume and the reducing agents of bacterial culture (See supplemental information). The influence of ΣH_2S released from the decomposition of cysteine in yeast extract and Na-thioglycolate on the $^{34}\varepsilon_{SR}$ values is minimal and is discussed in the supplemental information.

As for the decrease of csSRR according to the shift of growth phase and cell states, there are two possible cases. One is the case that almost all the cells in the cultures decreased their SRR in a similar manner likely due to the depletion of electron donor. The other is the case that most of the cells ceased the sulfate reduction activity but only a limited number of acclimated cells under the varying conditions kept the high sulfate reduction. The microscopic observation of cell morphology indicated that the cell size in our experiments gradually decreased in a similar manner from the exponential and the stationary phases of growth (Fig. 5). This implies that the decrease of total sulfate reduction rate according to the varying growth phases results from the decrease of sulfate reduction rate in each cell.

4.3. Intracellular sulfur isotope fractionation mechanism of sulfate reducing bacteria

We carried out a model calculation according to Wing and Halevy (2014) to compare the results with other studies (Fig. 6). The relatively good fit of our results with the model indicates intracellular metabolite concentration shape the variation of the $^{34}\varepsilon_{SR}$ value (Wing and Halevy, 2014). However, the $^{34}\varepsilon_{SR}$ values of the experimental results of this

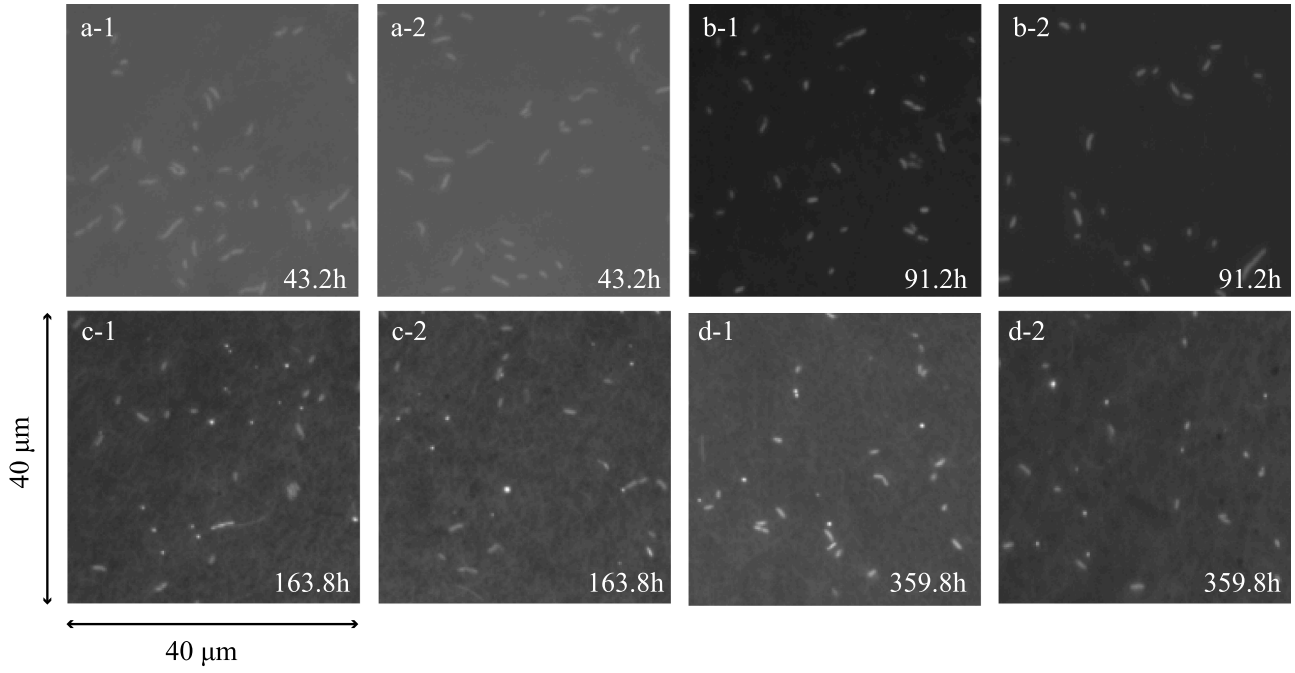

Fig. 5. Fluorescence photomicrograph of *D. desulfuricans* in various growth phase and states. (a) Cells at 43.2 h of series-1 experiment. (b) Cells at 91.2 h of series-1 experiment. (c) Cells at 163.8 h of series-2 experiment. (d) Cells at 359.8 h of series-2 experiment. The sizes of all pictures are 40 × 40 μm. The cell size gradually decreased from the early exponential phase to the stationary phase.

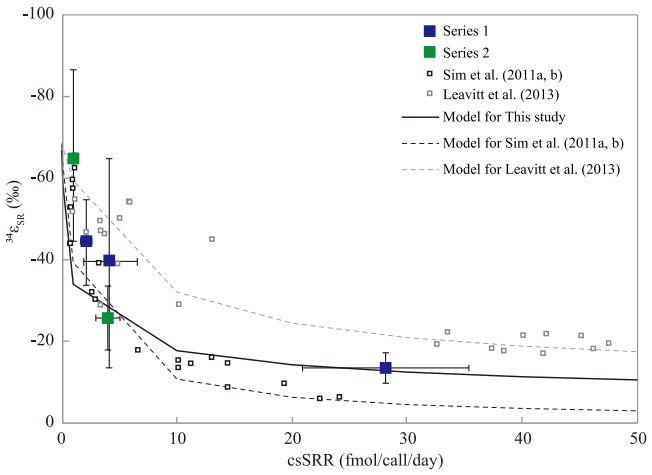

Fig. 6. Steady state model calculation according to Wing and Halevy, (2014). We applied scaling factor of 2.1 × csSRR + 70.0 for the calculation of the model of this study because the model with the value best fitted our results. The outer sulfate concentration, ΣH_2S concentration, and temperature were fixed to 16.0 mM, actual experimental values, and 30 °C, respectively for the calculation of this study. The model calculation for the data of Leavitt et al. (2013) and Sim et al. (2011a, 2011b) are from Wing and Halevy, (2014).

study at low csSRR area are high compared to those of the model (Fig. 6). Two possibilities can be considered to account for the discrepancy.

The first possibility is inconsistency of calculated intracellular metabolite concentrations with those of actual cells. The deviation of the data in this study from the model at low csSRR area may be attributed to low intracellular ΣH_2S concentration assumed for the model calculation. Wing and Halevy (2014) assumed the intracellular and extracellular ΣH_2S concentrations are equal and showed that model results are sensitive to the intracellular ΣH_2S concentration. The extracellular ΣH_2S concentration was set to 1 mM and c.a. 0.1 mM for the models of Leavitt et al. (2013) and this study, respectively (Fig. 6). Thus, if low csSRRs resulted in the buildup of intracellular ΣH_2S in the experiment of this study, the calculated $^{34}\varepsilon_{SR}$ value by the model of this study become higher and may align well with the data at low csSRR area. Besides, Sim et al. (2017) showed from the experiments of extracting intracellular metabolites of sulfate reducing bacteria that ratio of intracellular sulfite to APS is low compared to the model. Sim et al. (2017) suggested the discrepancy is likely owing to the employment of high redox potential electron carrier—menaquinone—in the model calculation and employing a low redox potential electron carrier may cancel the discrepancy between the experimental results and the model.

The second possibility is that the $^{34}\varepsilon_{SR}$ value is determined only from the isotopic composition of intracellular sulfate (Sim et al., 2017). Sim et al. (2017) showed intracellular sulfate was not accumulated and had high $\delta^{34}S$ value (+48.7‰) during the middle exponential phase of cells owing to high sulfate reduction rate. On the other hand, intracellular sulfate was accumulated and had low $\delta^{34}S$ value of +5.3‰ in the later exponential to stationary phases cells. They interpreted the change of the $\delta^{34}S$ value of intracellular sulfate resulted from a closed system effect owing to the change of sulfate reduction rate, and sulfur isotope fractionation during intracellular sulfate reduction to ΣH_2S always accompanies large isotope fractionation over 50‰. If this is the case, the $^{34}\varepsilon_{SR}$ value should not follow the calculation of steady state models including Wing and Halevy (2014), and our experimental results should not fit with the model (Fig. 6). Further experimental quantification of, and isotope analyses of intracellular metabolites seems to be a powerful way to elucidate the mechanism of intracellular sulfur isotope fractionation of microbial sulfate reduction.

4.4. The ΣH_2S-consuming reaction in stationary phase

We observed the decreasing ΣH_2S concentration during the stationary phase, which involves large sulfur isotope fractionations, $^{34}\varepsilon_{St} = -10.5 \pm 1.1$‰ and -45.6 ± 12.4‰, and decrease $\Delta^{33}S'_{H2S}$ values (Figs. 2B and 2C). Despite the large uncertainty, the $^{34}\varepsilon_{St}$ value in series-2 experiment must be larger than that of the series-1 experiment because of the steep increase in the slope of the linear regression in Fig. 2D, which may be owing to the shaking experimental condition. The lack of decreasing ΣH_2S concentration in the stationary phase of same experiments in Matsu'ura (2016b) is likely due to undetailed collection time and inaccurate quantification of ΣH_2S concentration. Further, we observed decreasing ΣH_2S in the cell-free experiment, which suggests the decrease in ΣH_2S concentration in the series-1 and series-2 experiments was not mediated by bacterial cells but mediated by non-microbiological reactions (Fig. 2A). Although the detail mechanism is still unidentified owing to the lack of identification of end-products, there are several possible explanations of non-microbiological reactions as follow.

One model is ΣH_2S oxidation with inorganic oxidants such as oxygen, iron, or manganese. However, this seems unlikely because the medium contains reducing agents such as ascorbic acid and Na-thioglycolate. In addition, the medium color was transparent throughout the experiment with resazurin indicator, which indicates contamination of oxygen into the medium was negligible.

The second model is precipitation as sulfide minerals. As mentioned in section 4.1, zinc sulfide was observed as the major sulfur-containing precipitates even in uninoculated samples and increased in number and size throughout the incubation experiment (Figs. S4A-D). Further, a nickel sulfide was observed in the medium of the supplemental cell-free experiment after 504 h of H_2S injection (Fig. S4E). However, as discussed about $\delta^{34}S_{TS}$ in the exponential phase, the calculated amount of sulfur in these visible precipitates is trivial as compared to the decreased amount of ΣH_2S. In addition, for measurement of ΣH_2S isotope composition, we collected zinc sulfide precipitates from media including ΣH_2S (section 2.2). Thus, sulfide precipitates, especially zinc sulfide, during the incubation experiments were included in the measured values of ΣH_2S isotope composition.

Finally, we inspected the possibility of sulfurization of organic matter with ΣH_2S. It is well known that glucose as well as other organic matter is sulfurized with ΣH_2S in aquatic solution in ambient temperature and relatively short time scale (Amrani, 2014; Pohlabeln et al., 2017). We detected one visible (>10μm) sulfurized organic matter grain in the medium of series-3 experiment at 593 h using SEM (Fig. S4F), showing that organic matter sulfurization occurred in the incubation medium. The amount of sulfur in the organic sulfur grain was calculated as 9.0×10^{-11} mol assuming that the organic sulfur grain possesses a volume of $20^3 \mu m^3$ and is primarily composed of thiolane $(CH_2)_4S$. The calculated amount of the sulfur corresponds to 2.3×10^{-3} μM in our growth medium, which is 2 orders of magnitude lower than that of the zinc sulfide (0.45 μM). In addition, the decreasing rate of the ΣH_2S concentration was similar between the media with and without glucose (Fig. S3C). However, our incubation medium contains organic compounds other than glucose such as yeast extract and Na-thioglycolate. Besides, the majority of organic sulfur compounds exist in liquid form at our experimental condition. Thus, organic matter sulfurization may explain non-microbiological reaction of decreasing ΣH_2S concentration during the stationary phase but would be promoted by organic compounds other than glucose such as yeast extract and Na-thioglycolate in the medium.

In summary, we observed precipitates of sulfide minerals and organic sulfur as the possible sinks of the decreasing ΣH_2S concentration during stationary phase. However, the calculated sulfur amount in the observed grains of sulfide minerals and organic sulfur seemed to be not enough to account for the decreased ΣH_2S amount during the stationary phase. Nevertheless, there may be abundant invisible small grains and

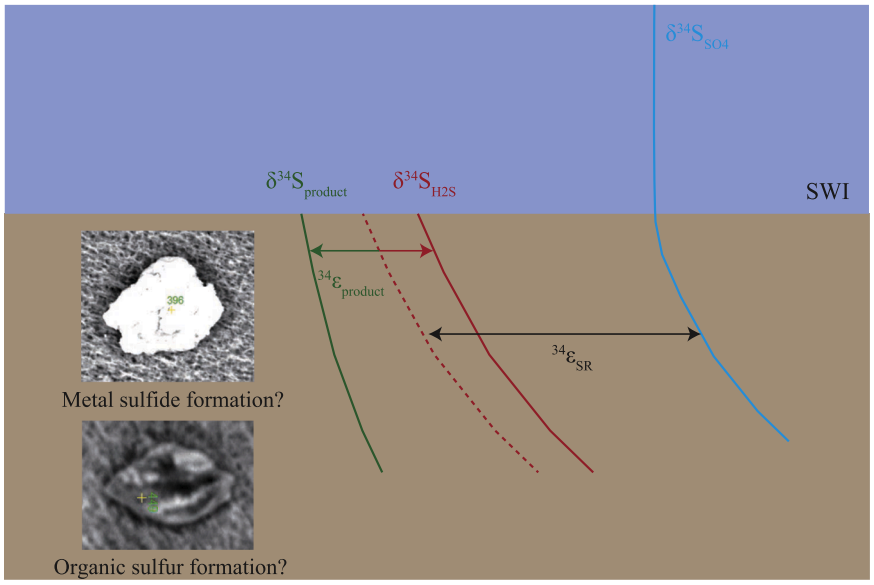

Fig. 7. Schematics of plausible sulfur cycling of some modern marine sediments in where ΣH_2S is accumulated. Blue line denotes $\delta^{34}S$ value of seawater and porewater sulfate. Red dotted and solid lines represent the $\delta^{34}S$ values of ΣH_2S generated through microbial sulfate reduction and modified by the ΣH_2S-consuming reaction, respectively. $^{34}\varepsilon_{SR}$ denotes sulfur isotope fractionation of microbial sulfate reduction same as defined in this study. Green line denotes $\delta^{34}S$ values of the products (metal sulfide or organic sulfur) of the ΣH_2S-consuming reaction. The $^{34}\varepsilon_{product}$ denotes sulfur isotope fractionation of the ΣH_2S-consuming reaction, which is equal to $^{34}\varepsilon_{st}$ in this study. The pictures of nickel sulfide and organic sulfur are from Fig. S4. SWI denotes sediment water interface.

dissolved forms of both inorganic and organic sulfur materials in the medium during the stationary phase. Although the detail mechanism is still uncertain, it seems likely that non-microbiological consumptions of ΣH_2S during the stationary phase by minerals and organic matter decreased the amount of accumulated ΣH_2S produced by sulfate reducing bacteria.

4.5. Implication for natural environments

The results of this study reinforce the importance of cell growth phase and states on $^{34}\varepsilon_{SR}$ value in natural environments. The csSRR in natural oceanic sediments is controlled by the organic matter flux to the sediments (D'Hondt et al., 2002); however, the csSRRs observed in this study and previous incubation experiments (10^{-1} to 10^{2} fmol/cell/day) are logarithmically higher than those observed in the natural environments (10^{-7} to 10° fmol/cell/day), which hesitate us to apply results of incubation experiments to elucidate the sulfur cycling of natural environments (Jørgensen 2021; Turchyn and Druhan, 2022). Indeed, Masterson et al. (2022) indicated the $^{34}\varepsilon_{SR}$ value in marine sediments is always ca. -70‰ regardless of the flux of organic matter as well as methane, and csSRR in marine sediments is always lower than that achieved in incubation experiments. One of the exceptional sites for the consistent $^{34}\varepsilon_{SR}$ value in natural environments are microbial mats and methane seep sediments where copious amount of organic matter or methane load increase csSRR and decrease the extent of $^{34}\varepsilon_{SR}$ value (Habicht and Canfield, 1997; Gong et al., 2018).

In addition to the microbial sulfur isotope fractionation, we showed non-microbiological isotope fractionations by ΣH_2S-consuming reaction in the stationary phase, $^{34}\varepsilon_{St}$ = -10.5 ± 1.1‰ and -45.6 ± 12.4‰ (Fig. 2), which are likely owing to the precipitation of acid insoluble sulfide minerals or sulfurization of organic matter. In both cases, the product has lower $\delta^{34}S$ value compared to ΣH_2S and increase $\delta^{34}S_{H2S}$ value in where hydrogen sulfide is accumulated in water column or sediments. In particular, high $\delta^{34}S_{H2S}$ value compared to that of coexisting pyrite or organic sulfur was reported in several modern marine sediments (Werne et al., 2003; Raven et al., 2016). Raven et al. (2016) reported the $\delta^{34}S_{H2S}$ value in Santa Barbara Basin porewater is uniformly 5–30‰ higher than that of coexisting pyrite and interpreted that the pyrite with low $\delta^{34}S$ value (-30 to -40‰) was formed in microenvironments such as microbial aggregates or biofilms. This interpretation is based on the observation that equilibrium isotope fractionation between most metal sulfides and ΣH_2S is negligible and occurs in the opposite direction ($\delta^{34}S_{product} > \delta^{34}S_{H2S}$) (Seal, 2006). A large kinetic isotope fractionation is necessary to produce metal sulfide with a lower $\delta^{34}S$ value compared to that of ΣH_2S. Although Böttcher et al. (1998) demonstrated the occurrence of kinetic isotope fractionations in the normal direction during iron-sulfide precipitation from ΣH_2S, the sulfur isotope fractionations are minimal, approximately -3‰. In addition to the metal sulfide, Raven et al. (2015) showed that the $\delta^{34}S$ values of some organic sulfur species in the sediments of Cariaco Basin are lower than those of the coexisting ΣH_2S nadir to -43.6‰, which is *ca* 14‰ lighter than the coexisting ΣH_2S. Besides, the $\delta^{34}S$ values of the organic sulfur is lower than the coexisting pyrite (chromium reducible sulfur) whose $\delta^{34}S$ value is about -33‰. These low $\delta^{34}S$ value of organic sulfur was enigmatic because no large kinetic isotope effect has been reported for organic matter sulfurization (Raven et al. 2015). Furthermore, when considering the pyrite and organic sulfur were formed from same ΣH_2S pool, organic matter sulfurization is expected to involve a larger kinetic isotope effect than pyrite formation in the sediments of Cariaco Basin. Raven et al. (2015) proposed the kinetic isotope effect during organic matter sulfurization is a consequence of the irreversible reaction between HS^- (bisulfide) and organic matter, leading to the formation of thiol, instead of the reversible reaction between S_x^{2-} (polysulfide) and organic matter, leading to the formation of sulfur catenation. Assuming the reaction occurring in the stationary phase of this study involves organic matter sulfurization with a kinetic isotope effect, this could account for the observed low $\delta^{34}S$ values in organic sulfur within Cariaco Basin sediments (Fig. 7). At the same time, the formation of organic sulfur species with low $\delta^{34}S$ value increases the $\delta^{34}S$ value of ΣH_2S, potentially explaining the higher $\delta^{34}S_{H2S}$ values observed compared to those of coexisting pyrite in some modern marine sediments. Large kinetic isotope fractionation observed in the stationary phase cells of our study is necessary to account for the elevated $\delta^{34}S_{H2S}$ values observed in some modern marine sediments including Cariaco Basin. Identification of the end-product of the reaction of the stationary phase in this study is necessary for further discussion.

5. Conclusion

Two series of pure culture incubation experiments of a type sulfate reducing bacterium, *D. desulfuricans*, were carried out from the early exponential phase to the stationary phase. The magnitude of the $^{34}\varepsilon_{SR}$ values increased from -13.4 ± 3.6‰ in the early exponential phase to -65.9 ± 21.0‰ in the later exponential phase concomitant with the decrease of csSRR from 28.1 ± 7.2 to 1.0 ± 0.3 fmol/cell/day. The decrease of csSRR is likely owing to the increase in the small cells with low sulfate reduction rate. The large variation of $^{34}\varepsilon_{SR}$ value shows the importance of cell's growth phase and states. The shift of cell growth phase likely changed the concentration and isotopic composition of intracellular sulfur species, which control the exerted $^{34}\varepsilon_{SR}$ value. At the same time, we observed inconsistency of isotopic composition of total sulfur and discrepancy of decreased sulfate and increased ΣH_2S concentration in the exponential phase, which indicate the existence of unidentified intracellular or extracellular sulfur species. In addition to the large variation of the $^{34}\varepsilon_{SR}$ value, our study first report decreasing ΣH_2S concentration during the incubation experiment of sulfate reducing bacteria. Besides, the ΣH_2S-consuming reaction in the stationary phase accompanied large sulfur isotope fractionations, $^{34}\varepsilon_{St}$ = -10.5 ± 1.1‰ and -45.6 ± 12.4‰, and decreased $\Delta^{33}S'_{H2S}$ values. Although the detail mechanism is still unidentified owing to the lack of identification of end-products, we observed precipitate of some sulfide minerals and organic sulfur in the incubation medium of the stationary phase. Since there is no known ΣH_2S-consuming reaction which involves large negative sulfur isotope fractionation and increase $\delta^{34}S$ value of ΣH_2S, our finding can account for high $\delta^{34}S_{H2S}$ value compared to that of coexisting pyrite or organic sulfur reported in several modern marine sediments.

CRediT authorship contribution statement

Fumihiro Matsu'ura: Writing – original draft, Methodology, Investigation, Conceptualization. **Hiroko Makita:** Supervision, Methodology, Investigation. **Ken Takai:** Writing – review & editing, Supervision. **Mayuko Nakagawa:** Investigation. **Yuichiro Ueno:** Writing – review & editing, Investigation, Conceptualization.

Declaration of Competing Interest

The authors declare that they have no known competing financial interests or personal relationships that could have appeared to influence the work reported in this paper.

Data availability

All experimental data in this study are attached in supplemental tables.

Acknowledgment

The authors are grateful to the associate editors, Prof. Boswell Wing and Prof. Laurence Coogan for handling this paper. Constructive comments by two anonymous reviewers helped improving the manuscript. We are grateful to Prof. Shawn McGlynn with the help of cell counting at Tokyo Tech. We are grateful to Nanjing University for their support of the corresponding author's travel for the experiments in revision stage conducted in Japan.

Supplementary materials

Supplementary material associated with this article can be found, in the online version, at doi:10.1016/j.epsl.2023.118446.

References

Amrani, A., 2014. Organosulfur compounds: molecular and isotopic evolution from biota to oil and gas. Annu. Rev. Earth Planet. Sci. 42, 733–768.
Bertran, E., Leavitt, W.D., Pellerin, A., Zane, G.M., Wall, J.D., Halevy, I., Wing, B.A., Johnston, D.T., 2018. Deconstructing the dissimilatory sulfate reduction pathway: isotope fractionation of a mutant unable of growth on sulfate. Front. Microbiol. 9, 3110.
Böttcher, M.E., Smock, A.M., Cypionka, H., 1998. Sulfur isotope fractionation during experimental precipitation of iron (II) and manganese (II) sulfide at room temperature. Chem. Geol. 146, 127–134.
Bradley, A.S., Leavitt, W.D., Schmidt, M., Knoll, A.H., Girguis, P.R., Johnston, D.T., 2016. Patterns of sulfur isotope fractionation during microbial sulfate reduction. Geobiology 14, 91–101.
Chambers, L.A., Trudinger, P.A., 1979. Microbiological fractionation of stable sulfur isotopes: a review and critique. Geomicrobiol. J. 1, 249–293.
Cline, J.D., 1969. Spectrophotometric determination of hydrogen sulfide in natural waters 1. Limnol. Oceanogr. 14, 454–458.
D'Hondt, S., Rutherford, S., Spivack, A.J., 2002. Metabolic activity of subsurface life in deep-sea sediments. Science 295, 2067–2070.
Davidson, M.M., Bisher, M.E., Pratt, L.M., Fong, J., Southam, G., Pfiffner, S.M., Reches, Z., Onstott, T.C., 2009. Sulfur isotope enrichment during maintenance metabolism in the thermophilic sulfate-reducing bacterium Desulfotomaculum putei. Appl. Environ. Microbiol. 75, 5621–5630.
Detmers, J., Brüchert, V., Habicht, K.S., Kuever, J., 2001. Diversity of sulfur isotope fractionations by sulfate-reducing prokaryotes. Appl. Environ. Microbiol. 67, 888–894.
Ding, T., Valkiers, S., Kipphardt, H., De Bievre, P., Taylor, P.D.P., Gonfiantini, R., Krouse, R., 2001. Calibrated sulfur isotope abundance ratios of three IAEA sulfur isotope reference materials and V-CDT with a reassessment of the atomic weight of sulfur. Geochim. Cosmochim. Acta 65, 2433–2437.
Gong, S., Peng, Y., Bao, H., Feng, D., Cao, X., Crockford, P.W., Chen, D, 2018. Triple sulfur isotope relationships during sulfate-driven anaerobic oxidation of methane. Earth Planet. Sci. Lett. 504, 13–20.
Habicht, K.S., Canfield, D.E., 1997. Sulfur isotope fractionation during bacterial sulfate reduction in organic-rich sediments. Geochim. Cosmochim. Acta 61, 5351–5361.
Johnston, D.T., 2011. Multiple sulfur isotopes and the evolution of Earth's surface sulfur cycle. Earth Sci. Rev. 106, 161–183.
Jørgensen, B.B., 2021. Sulphur biogeochemical cycle of marine sediments. Geochem. Perspect. 10, 145–146.
Kiba, T., Takagi, T., Yoshimura, Y., Kishi, I., 1955. Tin (II)-strong phosphoric acid. A new reagent for the determination of sulfate by reduction to hydrogen sulfide. Bull. Chem. Soc. Jpn. 28, 641–644.
Leavitt, W.D., Halevy, I., Bradley, A.S., Johnston, D.T., 2013. Influence of sulfate reduction rates on the Phanerozoic sulfur isotope record. Proc. Natl. Acad. Sci. 110, 11244–11249.
Leavitt, W.D., Venceslau, S.S., Waldbauer, J., Smith, D.A., Pereira, I.A.C., Bradley, A.S., 2019. Proteomic and isotopic response of Desulfovibrio vulgaris to DsrC perturbation. Front. Microbiol. 10, 658.
Masterson, A.L., Alperin, M.J., Arnold, G.L., Berelson, W.M., Jørgensen, B.B., Røy, H., Johnston, D.T., 2022. Understanding the isotopic composition of sedimentary sulfide: a multiple sulfur isotope diagenetic model for Aarhus Bay. Am. J. Sci. 322, 1–27.
Matsu'ura, F., Sunamura, M., Ueno, Y., Urabe, T., 2016a. Influence of cell's growth phase on the sulfur isotopic fractionation during in vitro microbial sulfate reduction. Chem. Geol. 431, 1–9.
Matsu'ura, F., 2016b. Sulfur Cycling in Ediacaran and Early Cambrian Periods Reconstructed from Quadruple Sulfur Isotope Analysis and Culture Experiment of Sulfate Reducing Bacteria. Ph. D. thesis, Tokyo Institute of Technology.
Ono, S., Wing, B., Johnston, D., Farquhar, J., Rumble, D, 2006. Mass-dependent fractionation of quadruple stable sulfur isotope system as a new tracer of sulfur biogeochemical cycles. Geochim. Cosmochim. Acta 70, 2238–2252.
Pellerin, A., Wenk, C.B., Halevy, I., Wing, B.A., 2018. Sulfur isotope fractionation by sulfate-reducing microbes can reflect past physiology. Environ. Sci. Technol. 52, 4013–4022.
Pellerin, A., Antler, G., Marietou, A., Turchyn, A.V., Jørgensen, B.B., 2020. The effect of temperature on sulfur and oxygen isotope fractionation by sulfate reducing bacteria (Desulfococcus multivorans). FEMS Microbiol. Lett. 367 fnaa061.
Pohlabeln, A.M., Gomez-Saez, G.V., Noriega-Ortega, B.E., Dittmar, T., 2017. Experimental evidence for abiotic sulfurization of marine dissolved organic matter. Front. Mar. Sci. 4, 364.
Raven, M.R., Adkins, J.F., Werne, J.P., Lyons, T.W., Sessions, A.L., 2015. Sulfur isotopic composition of individual organic compounds from Cariaco Basin sediments. Org. Geochem. 80, 53–59.
Raven, M.R., Sessions, A.L., Fischer, W.W., Adkins, J.F., 2016. Sedimentary pyrite δ34S differs from porewater sulfide in Santa Barbara Basin: proposed role of organic sulfur. Geochim. Cosmochim. Acta 186, 120–134.
Rees, C.E., 1973. A steady-state model for sulphur isotope fractionation in bacterial reduction processes. Geochim. Cosmochim. Acta 37, 1141–1162.
Santos, A.A., Venceslau, S.S., Grein, F., Leavitt, W.D., Dahl, C., Johnston, D.T., Pereira, I. A., 2015. A protein trisulfide couples dissimilatory sulfate reduction to energy conservation. Science 350, 1541–1545.
Seal, R.R., 2006. Sulfur isotope geochemistry of sulfide minerals. Rev. Mineral. Geochem. 61, 633–677.

Sim, M.S., Ono, S., Donovan, K., Templer, S.P., Bosak, T., 2011a. Effect of electron donors on the fractionation of sulfur isotopes by a marine Desulfovibrio sp. Geochim. Cosmochim. Acta 75, 4244–4259.
Sim, M.S., Bosak, T., Ono, S., 2011b. Large sulfur isotope fractionation does not require disproportionation. Science 333, 74–77.
Sim, M.S., Paris, G., Adkins, J.F., Orphan, V.J., Sessions, A.L., 2017. Quantification and isotopic analysis of intracellular sulfur metabolites in the dissimilatory sulfate reduction pathway. Geochim. Cosmochim. Acta 206, 57–72.
Stögbauer, A., Koydon, S., Berner, Z., Winter, J., Stüben, D, 2004. Effect of molybdate and cell growth on S-isotope fractionation during bacterial sulfate reduction. Geomicrobiol. J. 21, 207–219.
Turchyn, A.V., Druhan, J.L., 2022. The effects of reactive transport on sulfur isotopic compositions in natural environments. In: Sims, K.W.W., Maher, K., Schrag, D.P. (Eds.), Isot. Constraints Earth Syst. Process. American Geophysical Union, pp. 271–284.
Ueno, Y., Aoyama, S., Endo, Y., Matsu'ura, F., Foriel, J., 2015. Rapid quadruple sulfur isotope analysis at the sub-micromole level by a flash heating with CoF3. Chem. Geol. 419, 29–35.
Werne, J.P., Lyons, T.W., Hollander, D.J., Formolo, M.J., Damsté, J.S.S., 2003. Reduced sulfur in euxinic sediments of the Cariaco Basin: sulfur isotope constraints on organic sulfur formation. Chem. Geol. 195, 159–179.
Wing, B.A., Halevy, I., 2014. Intracellular metabolite levels shape sulfur isotope fractionation during microbial sulfate respiration. Proc. Natl. Acad. Sci. 111, 18116–18125.